PAPER

Check for updates

Structure and dynamics of an aqueous solution containing poly-(acrylic acid) and non-ionic surfactant octaethylene glycol *n*-decyl ether (C$_{10}$E$_8$) aggregates and their complexes investigated by molecular dynamics simulations†

Lakshmikumar Kunche and Upendra Natarajan (ID)*

A detailed molecular dynamics simulation study of the self-assembly, intermolecular structure and thermodynamic behavior of an aqueous solution of non-ionic surfactant octa ethylene glycol *n*-decyl ether (C$_{10}$E$_8$) in the presence of a non-ionic polar polymer poly(acrylic acid) PAA is presented. The aggregation number N_{agg} and concentration of surfactant C_s in the simulation systems were varied in the range 0.01–0.32 M and $5 < N_{agg} < 101$ (dilute to concentrated) with a dilute polymer concentration (C_p = 0.01 M). Lamellar aggregates of non-ionic surfactant in bulk aqueous solution are shown by molecular level computations for the first time. Spherical micellar aggregates and lamellar aggregates are formed at low and high N_{agg}, respectively. The transition from the spherical micelle phase to the lamellar phase in a binary solution is captured for the first time. A conformational transition from coiled to extended PAA chains adsorbed on the surfactant aggregate occurs at a particular value of N_{agg}, commensurate with the transition from spherical micelle aggregates to anisotropic lamellar aggregates. Formation of the surfactant aggregate in binary and ternary solutions and the polymer–surfactant complex in a ternary solution is enthalpically favored. Adsorption of PAA on the surfactant aggregate surface is driven by hydrogen bonds (HBs) between carboxylic acid groups of PAA and ethylene oxide groups of C$_{10}$E$_8$. A significant number of HBs occur between polar oxygens of C$_{10}$E$_8$ and hydroxyl oxygens of PAA. The results are in agreement with the limited available experimental data on this system.

1. Introduction

Liquid mixtures containing polymers and surfactants are important in applications such as detergents, cosmetics, pharmaceutical chemicals, paints, adhesives, coating fluids, oil recovery fluids, emulsion polymerization, rheological modifiers, stabilization of protein membranes, and surface engineering.[1–9] While extensive studies of charged polymers and ionic surfactants in aqueous solution have attracted considerable attention, those of uncharged polymers and non-ionic surfactants are fewer. The interactions between polar polymers and non-ionic surfactants are dominated by dispersion forces and hydrogen bonding between polar moieties of the surfactant and the polarizable groups of the polymer.[10,11] Spherical aggregates at lower

Macromolecular Modeling and Simulation Lab, Department of Chemical Engineering, Indian Institute of Technology (IIT) Madras, Chennai 600036, India.
E-mail: unatarajan@iitm.ac.in; Fax: +91-44-22574150, +91-44-22574152;
Tel: +91-44-22574184
† Electronic supplementary information (ESI) available. See DOI: 10.1039/d0sm01322f

concentration, and symmetric and asymmetric lamellar aggregates at higher concentration are formed in aqueous solutions of nonionic surfactants.[9,12,13] Aggregates comprising polymer chains and surfactant molecules in ternary (polymer–surfactant–water) solutions are formed at the critical aggregate concentration (denoted as CAC or T_1) below the critical micelle concentration CMC of the surfactant–water binary solution. The formation of free micelles occurs at the "free-micelle" concentration (denoted as T_2, where T_2 is greater than the CAC) in ternary polymer–surfactant–water solutions.[1,2] Apart from spherical micelles, non-ionic surfactants form several mesophases such as spherical micelles, hexagonal, normal-cubic-bicontinuous, lamellar, and reversed-cubic-bicontinuous. Large head-groups and low temperature favor the formation of spherical micelles and the hexagonal phase while the lamellar and reverse cubic phases are favored by small head-groups at higher temperature.[9,12,13]

Surfactants can be non-ionic or ionic. The interactions between non-ionic surfactants and polymers, such as PAA–C$_m$E$_n$ and PMA–C$_m$E$_n$, where m denotes the number of CH$_2$

groups (C) present in the aliphatic part and n denotes the number of ethylene oxide (EO) groups in the hydrophilic part (E), have been investigated by experimental techniques such as fluorescence quenching,[14,15] surface tension measurements,[11,15–17] calorimetry,[18] dye solubilization,[15] and viscometry.[15,17] The surface tension of an aqueous solution reduces with an increase in the surfactant concentration up to a critical concentration value, beyond which it remains constant.[1,3,4] The hydrophobic CH_2 groups present in the alkyl part of the surfactant are responsible for the reduction in the excess free energy of the water surface, thereby reducing the surface tension. Measurements of the surface tension of an aqueous solution of a surfactant by tensiometry[16,18] provide an easy method to determine the CMC as well as the area per surfactant molecule at the CMC. However, the necessary information on T_1 and T_2 in polymer–surfactant–water solutions can be provided only by calorimetry[18] and spectrofluorometric measurements.[17]

The intermolecular interactions between anionic polyelectrolyte poly(acrylic acid) PAA and C_mE_n type non-ionic surfactants in aqueous solution are sensitive to pH.[11,16,17,20] At low pH, PAA is neutral (acidic) as all carboxylic acid groups are protonated. At higher pH > 3.25 the PAA chains are converted to anionic species by deprotonation of COOH groups, which results in enhancement of the hydrogen bonding between the polymer and the surfactant and between the polymer and water. Surfactants containing a longer hydrophilic (EO) part tend to interact strongly with anionic polymers such as PAA.[11] For pH > 5 the interaction between the polymer and the surfactant is reduced due to significant electrostatic repulsion between carboxylate groups of the polymer and EO groups of the surfactant.[20] The pH range for strong favorable polymer–surfactant intermolecular association in the case of PAA–$C_{12}E_8$ aqueous solution is 3–5.[16] The values of the critical concentrations CAC and CMC decrease with an increase in the length m of the hydrophobic alkyl chain.[16] Experimental studies[16] of surfactant series C_mE_8 (m = 10, 12, 14) have shown that the surfactant having a longer tail shows a lower value of the CMC and CAC. In the surfactant series having the same length of the hydrophobic tail but different hydrophilic lengths, the value of T_1 is the same but the value of T_2 is lower for a surfactant having a longer hydrophilic part.[17] Interestingly, experimental studies[21] involving a comparison between poly(acrylic acid) PAA and poly(methacrylic acid) PMA with $C_{12}E_6$ and $C_{12}E_8$ surfactants have shown that T_1 > CMC in the case of PMA whereas T_1 < CMC for PAA. The influence of the polymer molecular weight on the strength of the polymer–surfactant interaction has been investigated specifically by an extensive study taking the example of PAA–C_8E_5–water solution.[19] The value of T_1 is independent of the polymer molecular weight T_1, whereas the free-micelle concentration T_2 is less for a solution containing a polymer of lower molecular weight (<1×10^5 Da) and remains constant beyond 1×10^5 Da. The cloud point temperature of the solution increases with the number of EO groups.[22]

Surfactants self-assemble to form structured aggregates to avoid thermodynamically unfavorable intermolecular contacts

in aqueous solution.[23–26] The hydrophobic CH_2 of the alkyl tail increases the excess free energy of the water surface, thereby reducing the surface tension.[24] The intra-micellar structure of ionic surfactants in aqueous solution has been studied extensively using molecular dynamics simulations.[27–37] Molecular simulation studies of surfactant aggregates and surfactant assemblies at interfaces and of polymer–surfactant self-assembly in solution using atomistic scale, coarse-grained, and dissipative particle dynamics have been reviewed and summarized.[29] Different micelle morphologies such as bottle brushes, swollen cages and necklace formations[30] have been shown by Dissipative Particle Dynamics (DPD) simulations of model surfactants in solution.

The seminal model of Nagarajan and Ruckenstein[38–40] based on molecular theory provides the free-energy of aggregation and size distribution of aggregates of ionic and non-ionic surfactant molecules in aqueous solution. The prediction of the CMC, shape and size of micelles of model ionic and nonionic surfactants in solution is possible using the molecular theory model.[39] The necklace-model of polymer–surfactant complexes and the statistical thermodynamics approach[41–44] are useful for the prediction of the critical aggregate concentration, the number of micelles bound to a polymer chain, the aggregation number of micelles bound to a polymer chain, the average distance between micelles in solution, and the mean-squared end-to-end distance of the polymer–surfactant complex aggregates.[43]

In most of the previous atomistic simulation studies of surfactants involving explicit chemistry (*i.e.* real chemical systems)[31,45,47] the initial configurations of surfactant molecules were taken as the loosely packed pre-assembled micelle form, as these preassembled micelles require less computational time to equilibrate to the final aggregate. However, the use of pre-assembled micelles is not an appropriate way to study new systems or to unequivocally establish the formation of aggregates. The only available atomistic simulation studies on the structure of aggregates of non-ionic surfactants in aqueous solution are those using the pre-assembled micelle approach.[31,45,47] To our knowledge, no studies are available on realistic explicit chemistry based models of aqueous solutions of water soluble polymers and non-ionic surfactants which have looked at structural, dynamic and thermodynamic properties. Despite current understanding of polymer–surfactant mixtures in solution obtained from experimental studies, the structural characterization and behavioral aspects of polymer–surfactant aggregates at the molecular and mesoscale are lacking. For systems in which either or both the polymer and surfactant are ionic (*i.e.* charged), atomistic scale molecular dynamics simulations[45–47] have provided molecular insights into the structure of the micelle core, polymer adsorption on the micelle surface, the penetration of water inside the hydrocarbon core, and the shape of the micelle. To the best of our knowledge, there are no existing studies of atomistic molecular simulations of aqueous solutions of water soluble polymers and non-ionic surfactants in the literature.

We present an atomistic and molecular simulation study of a realistic aqueous solution of explicit chemistry containing a non-ionic polar polymer, a non-ionic surfactant and water,

looking at the effect of the aggregation number and surfactant concentration on the intermolecular structure and thermodynamics of aggregation and the polymer–surfactant complex. This is also the first computational study which shows formation of lamellar surfactant aggregates of non-ionic surfactants in bulk aqueous solution and the key aspects of the structural behavior of such aggregates. This study, for the first time, shows the existence of a new transition (at a concentration or aggregation number) of the aggregate morphology, in going from a spherical micelle to a lamellar one, for systems consisting of non-ionic surfactants in binary (surfactant–water) and ternary (polymer, surfactant, and water) solutions. A new conformational transition of the polymer chains adsorbed on the surfactant micelle surface, which occurs at a particular aggregation number of the surfactant micelle, is observed for the first time in an aqueous solution containing a non-ionic polar polymer. It is difficult to probe such a transition *via* experiments. This transition is seen in the radius-of-gyration as well as in the thermodynamic contribution of the conformational changes of the polymer chain upon adsorption on the surfactant micelle.

The system studied in this work is the polycarboxylate type polar acidic polymer poly(acrylic acid) and the non-ionic surfactant octaethylene glycol *n*-octyl ether $C_{10}E_8$, over a wide range of surfactant concentration and aggregation number. Being a unique simulation study of atomistic explicit chemistry, this study brings out details not put forth by the earlier few DPD and MC studies in the literature. Several molecular aspects of the behavior of such a solution not easily obtained *via* experiments are brought out by this study. The initial arrangement of the surfactant molecules inside the simulation box is completely random, which makes our study more appropriate as compared to previous studies. The concentration of surfactant was varied from low to high in order to capture the different morphologies of the surfactant aggregates and polymer–surfactant complexes in aqueous solution. Multiple independent MD trajectories of sufficiently long times obtained from different starting conformations were used to sample the polymer conformations upon adsorption on the surfactant aggregate, by successfully sampling the configurational space. The structure of the morphologies is analyzed in detail using radial distribution functions, density profiles, and the solvent accessible surface area. The solvation thermodynamic properties of the binary system and ternary system are described by calculation of the enthalpy of solvation, aggregate formation and specific interactions, in binary and ternary solutions. The hydrogen bonding between the polymer and surfactant molecules is analyzed. Computational details of this study are given in the methodology section. The results and discussion section includes structural aspects of the surfactant aggregates and polymer chains and of the polymer–surfactant aggregates, and an analysis of the intermolecular structure through radial distribution functions, shape factor analysis, density profiles, hydrogen bonding, surface area analysis, and the chain conformations and chain dimensions of the polymer. The results are compared with experimental data. The final section provides a summary of the key conclusions of this study.
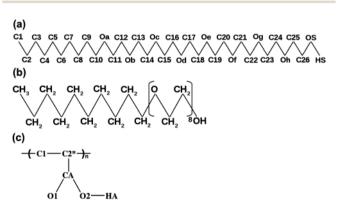
2. Methodology and computational details

2.1. Force-field and chain structure parameters

The distribution of surfactant molecules, polymer chains and water molecules was spatially uniform with random orientation and conformations for the initial configuration of the systems. The use of random configurations and spatial arrangement of molecules in the initial configuration for the MD runs bears the disadvantage that it takes a longer computational time to equilibrate, but provides realistic sampling as compared to the pre-assembled configurations[31,45,47] used in previous studies.

Potential energy minimization and MD simulations in the *NVT* and *NPT* ensembles were carried out using GROMACS version 4.0.7,[48] with the GROMOS 45a3 generic force-field (Fig. 1).[49] The aliphatic CH_2 and CH groups in the PAA chain and the $C_{10}E_8$ surfactant chains were treated as united atoms and the rest were treated explicitly. Reports in the literature have shown that the implementation of the GROMOS96 45A3 force-field gives a good agreement of the values of thermodynamic properties with experiments for hydrocarbons, poly-(acrylic acid),[45,49,50] and PEO.[47] The use of the GROMOS96 45A3 force-field also gives the correct hydrogen bonding of carboxylic acid polymers such as PAA and PMA in aqueous solution.[51–56] The GROMOS96 generic force-field is appropriate for molecular dynamics simulations of polar polymers and certain polyelectrolytes in aqueous solution.[50,57,58] Previous simulation studies in which the GROMOS96 45A3 force-field was used have shown results in good agreement with results obtained from experimental studies for the adsorption of non-ionic and ionic PAA on DTAC cationic surfactant micelles[45] and for polyethylene oxide–SDS complexation.[47] Therefore, the GROMOS96 45a3 force-field was chosen for carrying out the simulations in this study. The force-field parameters of PAA and the $C_{10}E_8$ surfactant are provided in Tables 3S and 4S, respectively, in the ESI.† The initial configurations of surfactants and polymer chains with random torsion angles along the backbone were generated using the Material Studio Visualizer interface.[59]

The torsion angle potential about the aliphatic backbone bonds in the polymer and surfactant was described by the

Fig. 1 (a) Chemical structure of $C_{10}E_8$. (b) Chemical structure of $C_{10}E_8$ with the atom description. (c) Repeat unit of PAA. * refers to chiral carbon.

Ryckaert–Bellemans functional form.[60] The van der Waals dispersion interactions and electrostatic interactions were modeled using the 6-12 Lennard-Jones potential function and the Reaction Field method,[61] respectively. The dielectric constant of the solution was kept constant and equal to 80 for all the systems in this study.

First, a polyethylene oxide (PEO) chain of 12 repeat units was simulated in aqueous solution at a temperature of 300 K and pressure of 1 bar. The value of $\langle R_g \rangle$ of this PEO chain obtained using the GROMOS96 45a3 force-field is 0.76 nm, in agreement with results from experiments as well as previous simulation studies performed under the same conditions.[47,62] This validated the use of the GROMOS96 45a3 force-field for simulations of PEO based surfactants in aqueous solution. The partial charges for oxygen atoms and the neighboring carbon atoms present in the polar EO group of the surfactant molecules were taken from a previous study of PEO chains in water.[47] A partial charge of $-0.5e$ was taken on this oxygen atom and $0.25e$ was taken for carbon atoms bonded to this oxygen atom.

2.2. Simulations of a binary solution: $C_{10}E_8$–water

The system specifications and simulation parameters are given in Tables 1 and 2. The concentration of surfactant molecules in the periodic simulation box was varied from 0.016 mol l^{-1} to 0.32 mol l^{-1}, which is higher than the range 8×10^{-5} to 10^{-2} mol l^{-1} used in experiments in bulk solution.[16] The edge length of the periodic cubic simulation box was fixed at 8 nm for systems containing up to 53 molecules (i.e. $N_{agg} \leq 53$, $C_s \leq 0.17$ mol l^{-1}) and an edge length of 10 nm was used for systems containing 61 to 101 molecules (i.e. $61 \leq N_{agg} \leq 101$ or 0.19 mol l$^{-1} < C_s < 0.32$ mol l^{-1}). The aggregation number N_{agg} is the number of surfactant molecules present in an aggregate. In order to observe the possibility of multiple micelles, the simulations were also carried out in a larger box of edge length 13 nm, as multiple micelles did not form in 8 nm and 10 nm boxes. Even in simulations of 101 molecules carried out in a 13 nm box a single lamellar aggregate is observed.

The simulation box was solvated with water molecules at each value of C_s. The SPC water model, a standard model for bulk water at ambient temperature, accepted for description of aqueous systems, was used in this study.[63–65] Studies[66] have shown that the SPC model can be successfully used for simulations of solutes in water in agreement with experimental results. The SPC water model is an accepted water model for use in simulations of synthetic polar polymers in aqueous solution.[50,67,68] A comparison was made of the conformational properties of fully-ionized PAA chains in water, as obtained using different combinations of force fields and water models, in a recent MD simulation study of PAA in aqueous solution.[69] The conclusion from that study was that the use of the GAFF

Table 1 Specifications of the systems

C_s (gmol l^{-1})	Box size (nm)	N_{agg}	Runs	Time (ns) t_{run}	Time (ns) t_{samp}	Time (ns) t_{eq}	No. of water molecules
0.016	8	5	2	70	60–70	55–70	16 863
0.042	8	13	2	60	50–60	45–60	16 598
0.068	8	21	2	60	50–60	45–60	16 350
0.094	8	29	2	60	50–60	45–60	16 083
0.12	8	37	2	60	50–60	45–60	15 832
0.14	8	45	2	60	50–60	45–60	15 574
0.17	8	53	2	60	50–60	45–60	15 324
0.19	10	61	2	60	50–60	45–60	31 172
0.22	10	69	2	60	50–60	45–60	30 906
0.25	10	77	2	60	50–60	45–60	30 645
0.27	10	85	2	40	35–40	30–40	30 387
0.30	10	93	2	60	50–60	45–60	30 134
0.32	10	101	2	60	50–60	45–60	29 882

Table 2 Simulation, equilibration and sampling times at various concentrations

C_s (gmol l^{-1})	No. of MD runs per system	Simulation time (ns)	Sampling time (ns)	Equilibration time (ns)
0.016	2	70	60–70	55–70
0.042	2	60	50–60	45–60
0.068	2	60	50–60	45–60
0.094	2	60	50–60	45–60
0.12	2	60	50–60	45–60
0.14	2	60	50–60	45–60
0.17	2	60	50–60	45–60
0.19	2	60	50–60	45–60
0.22	2	60	50–60	45–60
0.25	2	60	50–60	45–60
0.27	2	40	35–40	30–40
0.30	2	60	50–60	45–60
0.32	2	60	50–60	45–60

force field along with the SPC/E water model (parameters derived from the *ab initio* RESP charge fitting method) can accurately predict conformational properties such as the radius-of-gyration (R_g) and end-to-end distance (R) of charged PAA chains in aqueous solution in agreement with experimental values.[69] The use of the Gromos53a6 force field along with the SPC/E water model slightly over-predicts the values of R_g and R of the fully-ionized PAA chain by about 5%. However, such comparisons for uncharged PAA chains in aqueous solution are not available in the literature. The combination of the GROMOS96 force field along with the SPC water model gives the correct values of the radius of gyration of unionized PAA chains, as known from previous atomistic MD simulation studies.[50,52] Therefore, the GROMOS96 force field along with the SPC water model was implemented in this study. The use of the four-site TIP4P water model leads to a significant increase in computational cost, so it was not chosen for this study.

For the first set of simulations (denoted set-I), a coiled initial conformation was taken for surfactant molecules in all systems. For the second set of simulations (denoted set-II), an extended initial conformation was taken for surfactant molecules. Thus, the simulations for each system were carried out with two completely different initial conformations and orientations of the surfactant molecules and polymer chains, for obtaining appropriate sampling and time-averaging of properties. Simulations of the precise experimental concentration conditions were not possible due to the requirement of a periodic simulation box of very large dimensions beyond the scope of the computational resources for carrying out atomistic simulations.

The solvated PAA–$C_{10}E_8$ systems were subjected to energy minimization using the steepest descent method with the convergence criterion of the maximum force on any atom in the system being less than 1000 kJ mol^{-1}, followed by *NVT* and *NPT* molecular dynamics each for 100 ps. The equilibration runs were carried out in the *NPT* ensemble, from which the final period of 10 ns was taken as the sampling time for analysis. For the analysis the coordinates were written after every 500 steps during the trajectory. The simulations were performed at 300 K and 1 bar. All systems were sampled for properties subsequent to establishment of equilibration of the potential energy and the radius-of-gyration of the surfactant molecules and polymer chains.

The cut-off distance for electrostatic interactions was taken as 2 nm and the cut-in and cut-off values for the van der Waals interactions were kept at 1.0 nm and 1.1 nm, respectively. The cut-in value is the distance at which the potential is shifted so that the value of the potential goes to zero at the cut-off distance using the shift function.[70] Trial simulations were carried out with cut-in and cut-off values for van der Waals interactions taken as 1.3 nm and 1.4 nm. These gave similar results to those using 1.0 nm and 1.1 nm. However, the use of longer cut-offs required more computational time for equilibration and sampling. Therefore, smaller values of the cut-offs were chosen for further simulations. Covalent bonds were constrained using the LINCS algorithm,[71] and accordingly a time step of 2 fs was used to integrate the equations of motion

using the leap-frog algorithm. The atom neighbor-list was updated after every 10 steps using a 1 nm neighbor list cut-off. The V-rescale (velocity rescaling)[72] and Berendsen algorithms[73] were used for the temperature and pressure coupling baths, respectively. The velocity rescaling thermostat is a Berendsen thermostat which has an additional stochastic term that ensures a correct kinetic energy distribution. The velocity rescaling thermostat produces a correct canonical ensemble and has the advantage of a first order decay of temperature deviations with no oscillations.[72] The velocity rescaling thermostat has been used for MD simulations of polymers and proteins in solution.[74,75] Temperature and pressure coupling time constants τ_t = 0.1 ps and τ_p = 0.5 ps, pertaining to the compressibility of water being 4.5×10^{-10} kPa^{-1}, were used for coupling to the temperature (T = 300 K) and pressure (P = 1 bar) baths, respectively.[73,76,77]

2.3. Simulations of a ternary solution: PAA–$C_{10}E_8$–water

A 30-repeat unit atactic (random occurrence of *meso* and *racemic* dyads) PAA chain of molecular weight 2160 Da was used for all simulations corresponding to the experimental system available in the literature.[18] Two different initial conformations of the PAA chain were taken for carrying out independent simulations: one with a coiled conformation and another with an all *trans* (extended) conformation. The tacticity sequence of the atactic PAA chain is given in Table 1S in the ESI.† The sequences were generated using Monte Carlo simulations with target Bernoullian statistics for achieving dyad and triad fractions for a vinyl polymer chain that is synthesized using free-radical polymerization in bulk solution.[78,79] These tacticity statistics have been used in recent computational studies on vinyl polymers in aqueous solution[50,52,67,68,80] and have been utilized widely in the field of computational polymer science of vinyl polymer chains.

The periodic simulation box containing surfactant molecules and the polymer was solvated with water. The water molecular geometry (*i.e.* internal degrees of freedom) was constrained using the SETTLE algorithm.[81] For the initial configuration of the system, the surfactant molecules and polymer chain were distributed and oriented randomly along with water molecules. In the first stage, the system was subjected to energy minimization using the steepest descent method with an upper limit of force-constraint of 1000 kJ mol^{-1} on each atom. In the next stage, *NVT* and *NPT* molecular dynamics simulations, each for 100 ps, followed by equilibration runs in the *NPT* ensemble, were carried out. The final 10 ns of the trajectory was chosen for sampling and time-averaging of properties. The atom coordinates were written after every 500 steps for the purpose of carrying out the analysis. All simulations were performed at a temperature of 300 K and pressure of 1 bar. The simulation run times and sampling times at each concentration are given in Table 1. All systems were sampled for properties subsequent to establishment of equilibration of the system potential energy and the radius-of-gyration of surfactant molecules and PAA chains. The systems simulated using a relatively large periodic box size took significantly more computational time to equilibrate.

3. Results and discussion

In order to check for artifacts in the simulations a distance length scale (l_c) was calculated as given by the relation $l_c = S_{agg} + 2 \times C_d$, where S_{agg} is the size of the aggregate and C_d is the cut-off distance for the intermolecular potential. For a spherical micelle $S_{agg} = 2R_{mic}$, where R_{mic} is the radius of the micelle, and for the lamellar aggregate $S_{agg} = d_{lam}$ or h_{lam}, the diameter or height, whichever is larger, of the approximately cylindrical aggregate. The simulations are valid without artifacts if l_c is smaller than the size of the simulation box. l_c at the highest and lowest concentration values (*i.e.* size of aggregates) at which lamellar aggregates form in the ternary and binary solutions was calculated. The calculations were done using visualization and atom coordinates, without having the need to average over the top and bottom surfaces and the width cross-section of the lamellar aggregate, by consideration of the maximum distance values in each case. In the ternary solution at $C_s = 0.094$ mol l^{-1} ($N_{agg} = 29$) the values are $S_{agg} = 3.8$ nm and $l_c = 6$ nm, which are less than the box size (8 nm). We calculated a hypothetical equivalent spherical aggregate that may have formed at these concentrations (*i.e.* aggregation numbers) by equating the volume of the lamellar aggregate to the volume of a sphere, to obtain the radius of a sphere, denoted as R_{mic}. The corresponding value of R_{mic} is 1.8 nm and the value of l_c using R_{mic} is 5.7 nm, which is also less than the size of the box (edge length 8 nm). Therefore, clearly, there are no artifacts in the simulation. At these higher aggregation numbers lamellar aggregates must form. Similarly, at $C_s = 0.32$ mol l^{-1} ($N_{agg} = 101$), the upper end of the aggregation number studied, the values obtained are: $l_c = 7.7$ nm by using the corresponding S_{agg} and 7.8 nm using the corresponding R_{mic}. The value of l_c in both cases is significantly less than the box size 10 nm. In the binary system at $C_s = 0.14$ mol l^{-1} (*i.e.* $N_{agg} = 45$) we get $S_{agg} = 3.8$ nm and $l_c = 6$ nm, which are smaller than the size of the simulation box (8 nm). The equivalent hypothetical spherical aggregate radius $R_{mic} = 2.1$ nm and $l_c = 6.4$ nm, which are smaller in value as compared to the box size (8 nm). At $C_s = 0.32$ mol l^{-1} (*i.e.* $N_{agg} = 101$) in the binary solution we obtain $S_{agg} = 5.6$ nm and $l_c = 7.8$ nm, which are smaller than the size of the simulation box (10 nm). For this the corresponding values are $R_{mic} = 2.8$ nm and $l_c = 7.8$ nm for the hypothetical equivalent spherical micelle, which are smaller than the size of the simulation box (10 nm). From these calculations it is clear that l_c is always smaller than the size of the simulation box, so that there are no artifacts in the simulations.
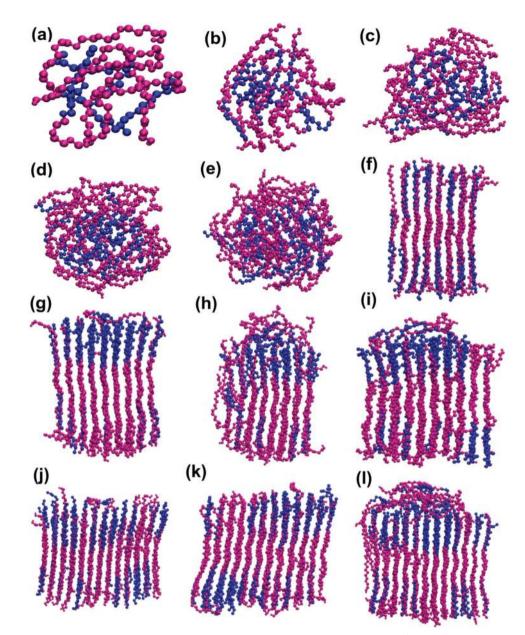
3.1. Binary $C_{10}E_8$–water solution

The specifications of the systems are given in Table 1. Snapshots of the equilibrated binary system are given in Fig. 2 and Fig. 1S and 2S as ESI.† The concentration of surfactant in the simulation box has a direct correspondence with the aggregation number of the micellar aggregate formed, as all surfactant molecules are part of the final micellar aggregate formed in the simulation. The concentration of surfactant molecules was varied in the range 0.016 mol $l^{-1} < C_s < 0.32$ mol l^{-1}. At low concentrations (range 0.016 mol $l^{-1} < C_s < 0.12$ mol l^{-1})

a single spherical micelle is formed and at higher concentrations (range 0.14 mol $l^{-1} < C_s < 0.32$ mol l^{-1}) lamellar aggregates are formed. Spherical aggregates and lamellar aggregates are formed below and above a critical value of the aggregation number, respectively. In order to observe the formation of multiple micelles additional simulations were carried out using a 13 nm box, but multiple micelles do not form and only a single lamellar aggregate is obtained. At $C_s = 0.016$ mol l^{-1} a single micelle is formed. The transition from the micelle phase to the lamellar phase is observed in the range 0.12 mol $l^{-1} < C_s < 0.14$ mol l^{-1}.

3.2. Ternary PAA–$C_{10}E_8$–water solution

Two independent simulations for each system were carried out with different initial conformations of the polymer: coiled and extended. The tacticity sequence of the polymer chain is given in Table 1S (ESI†). At a fixed value of the concentration of surfactant, the variation of the initial conformation of the polymer did not affect the final morphology of the aggregate. Snapshots of the ternary system are given in Fig. 3 and Fig. 3S and 4S (ESI†). The concentration of surfactant was varied in the range 0.016 mol l^{-1} to 0.32 mol l^{-1} (corresponding to the range of aggregation number $5 < N_{agg} < 101$). At lower values of C_s (range 0.016 mol $l^{-1} < C_s < 0.068$ mol l^{-1}; $5 < N_{agg} < 21$) spherical micelles are formed and at higher values (0.094 mol $l^{-1} < C_s < 0.32$ mol l^{-1}; $29 < N_{agg} < 101$) lamellar aggregates are formed. The concentration range, 0.016 mol $l^{-1} < C_s < 0.068$ mol l^{-1}, in which micelles are formed in the ternary system is slightly smaller as compared to the binary system (0.016 mol $l^{-1} < C_s < 0.094$ mol l^{-1}; $5 < N_{agg} < 29$) given that in the ternary system the presence of the adsorbed polymer chain would pose some difficulty to pack surfactants into a spherical micelle. At $C_s = 0.016$ mol l^{-1} the formation of micelles takes place in the binary and ternary solutions. Even at low concentration $C_s = 0.016$ mol l^{-1} the surfactant molecules interact with the polymer chain, in agreement with experimental data[17] on this system. The aggregates formed in the ternary solution clearly show the PAA chain adsorbed on the surface of the surfactant aggregate. This is driven by hydrogen bonding between the carboxylic acid groups of PAA and ethylene oxide groups of the surfactant.

3.3. Conformations of the polymer chain

The radius-of-gyration, R_g, of the PAA chain is shown in Fig. 4. The conformation of PAA is coiled at a lower concentration of surfactant (*i.e.* smaller aggregate size of the surfactant, spherical micelle regime) and extended at a higher concentration (*i.e.* larger aggregate size of the surfactant, lamellar micelle regime). $\langle R_g \rangle$ of PAA at the lowest surfactant concentration ($N_{agg} = 5$; $C_s = 0.016$ mol l^{-1}) is 0.79 nm, in agreement with the value in dilute aqueous solution obtained from previous studies.[50,53,69] As seen in Fig. 4 there is a clear transition in $\langle R_g \rangle$ of the PAA chain adsorbed on the aggregate, in going from the micellar regime to the lamellar regime. This transition occurs at $C_s = 0.09$ gmol l^{-1} (*i.e.* $N_{agg} = 24$). In the micellar regime PAA wraps around the surfactant micelle in a coiled conformation;
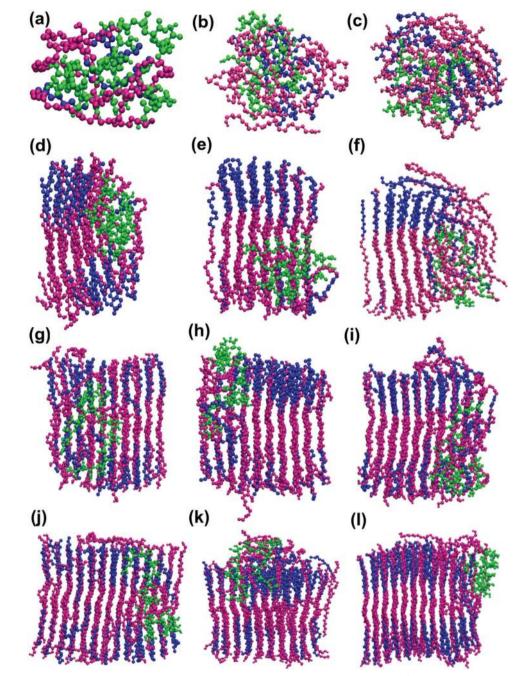
Fig. 2 Snapshots in the binary solution at different surfactant concentrations. (a) N_{agg} = 5, 0.016 gmol l^{-1}, (b) N_{agg} = 13, 0.042 gmol l^{-1}, (c) N_{agg} = 21, 0.069 gmol l^{-1}, (d) N_{agg} = 29, 0.094 gmol l^{-1}, (e) N_{agg} = 37, 0.12 gmol l^{-1}, (f) N_{agg} = 45, 0.14 gmol l^{-1}, (g) N_{agg} =53, 0.17 gmol l^{-1} (h) N_{agg} = 61, 0.19 gmol l^{-1}, (i) N_{agg} = 69, 0.22 gmol l^{-1}, (j) N_{agg} = 77, 0.25 gmol l^{-1}, (k) N_{agg} = 85, 0.27 gmol l^{-1}, and (l) N_{agg} = 101, 0.32 gmol l^{-1}. The magenta colour represents the polar moiety and the blue colour represents the non-polar moiety of the surfactant.

therefore, the value of R_g is low. The adsorption and coiling of the PAA chain on the micelle are driven by hydrogen bonding between carboxylic acid groups of PAA and EO groups of the $C_{10}E_8$ surfactant. For the lamellar aggregates, the polymer chain has to expand and extend itself to be able to adsorb in a site-specific manner for the interaction of COOH groups of PAA and EO groups of $C_{10}E_8$.

3.4. Size of the surfactant aggregate

The variation of the micelle radius (*i.e.* size of the micelle) with the concentration of surfactant is shown in Fig. 4. The size of the micelle increases with the aggregation number, which

changes with the surfactant concentration. At low concentration the PAA chain adsorbed on the aggregate surface holds the surfactant molecules together. However, at higher concentration the COOH interacting sites of the PAA chain are saturated with the EO groups of the surfactant molecules and PAA chain expansion and simultaneous enlargement of the aggregate occur. This leads to an increase in the surface area of the micelle with the surfactant concentration. The values of the intermolecular distance within the lamellar aggregate are given in Table 2S (ESI†). The intermolecular distance increases with the aggregation number, which implies that the size of the aggregate increases with the aggregation number. The intermolecular
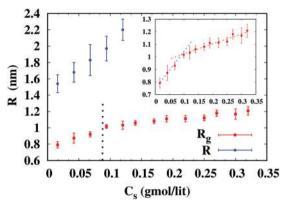
Fig. 3 Snapshots in the ternary solution at different surfactant concentrations. (a) N_{agg} = 5, 0.016 gmol l^{-1}, (b) N_{agg} = 13, 0.042 gmol l^{-1}, (c) N_{agg} = 21, 0.069 gmol l^{-1}, (d) N_{agg} = 29, 0.094 gmol l^{-1}, (e) N_{agg} = 37, 0.12 gmol l^{-1}, (f) N_{agg} = 45, 0.14 gmol l^{-1}, (g) N_{agg} = 53, 0.17 gmol l^{-1}, (h) N_{agg} = 61, 0.19 gmol l^{-1}, (i) N_{agg} = 69, 0.22 gmol l^{-1}, (j) N_{agg} = 77, 0.25 gmol l^{-1}, (k) N_{agg} = 85, 0.27 gmol l^{-1}, and (l) N_{agg} = 101, 0.32 gmol l^{-1}. The magenta colour represents the polar moiety, the blue colour represents the non-polar moiety of the surfactant and the green color represents the polymer chain.

distance is more in the case of aggregates in the binary solution as compared to the ternary solution, which shows the closer packing of the surfactant molecules in the presence of PAA. The values of d_{lam} and h_{lam}, the cross-section size and height of the cylinder approximately representing the lamellar aggregates in the binary and ternary solutions, are given in Table 2S of the ESI.† The d_{lam} values of the lamellar aggregate increase by a factor of 2 with an increase in concentration (*i.e.* aggregation number) from the lowest to the highest values, in the lamellar phase regime.

However, the h_{lam} value of the lamellar aggregate remains roughly constant across these aggregation numbers in the binary and ternary solutions.
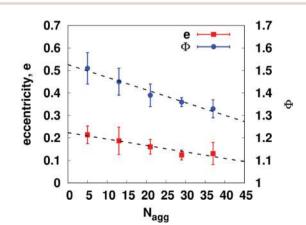
3.5. Geometry of micelles

The values of the aspect ratio (Φ) and the eccentricity (e) of the micelle (in the spherical micelle regime) were calculated using the standard relations[82] provided as eqn (S2) and (S3) in the ESI.† For a sphere, e = 0 and Φ = 1.[83] The geometry of the

Fig. 4 Average of the principal components of the radius-of-gyration $\langle R_g \rangle$ of the PAA chain averaged over MD run trajectories for two different tacticity sequences and the radius of the micellar aggregate R formed in the binary solution. The equation for the linear fit is $\langle R_g \rangle = 2.961 \times C_s + 0.7476$ in the micellar regime and $\langle R_g \rangle = 0.797 \times C_s + 0.944$ in the lamellar regime. The inset figure shows the variation of $\langle R_g \rangle$ of the PAA chain with the same axis labels as the main plot.

simulated $C_{10}E_8$ micelles was characterized using the aspect ratio (Φ) and eccentricity (e), which are shown in Fig. 5 and Fig. 5S and 6S of the ESI.† 20–30 ns were required to form a micelle of reasonable sphericity, as noted by the fluctuations of these geometric quantities in the MD trajectories. Linear fits of the simulated data of the eccentricity and aspect ratio, taking into consideration the fluctuations, gave the relations $e = (-0.0032 \pm 2 \times 10^{-6}) \times N_{agg} + (0.227 \pm 0.0016)$ and $\Phi = (-0.0054 \pm 4 \times 10^{-6}) \times N_{agg} + (1.518 \pm 0.0033)$. The detailed procedure for fitting a straight line to the data of the eccentricity and aspect ratio is provided in the ESI† (eqn (S12)–(S21)). The values of e and Φ show fluctuations in the range 0.15 to 0.25 and 1.3 to 1.5, respectively. These values show that the aggregate formed in the simulations corresponds to a spherical micelle.[83] Φ and e decrease with N_{agg}, which implies that the micelles are more spherical at higher C_s (or N_{agg}) in the spherical micelle regime. The values of Φ and e obtained for micelles in the binary solution are higher than those obtained in the ternary solutions, which shows that the
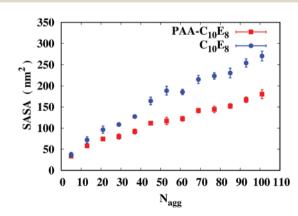
micelles simulated in the PAA–$C_{10}E_8$–water solution are more spherical than those simulated in the binary $C_{10}E_8$–water solution. This behavior occurs due to the presence of the PAA chain on the surface of the micelle, which binds with the surfactant molecules and keeps these together in an aggregate *via* favorable interactions between COOH groups of PAA and EO groups of $C_{10}E_8$.

3.6. Solvent accessible surface area (SASA)

The results for the solvent accessible surface area are presented in Fig. 6. The SASA was calculated using the DCLM method.[84] The SASA values of the micelles in the binary solution are greater than those in the ternary solution. In principle the three possible locations where the polymer chain can adsorb are: (i) on the surface of the micelle, (ii) on the hydrocarbon–water interface, and (iii) within the hydrocarbon core. Since simulations were carried out with the surfactant molecules placed randomly inside the simulation box in their initial configuration, there is equal *a priori* likelihood of the occurrence of any of these possibilities. As we have noted, the SASA values of aggregates formed in the binary systems are greater than the values in the corresponding ternary systems. Therefore, it is clear that the PAA chain adsorbs on the surface of the micelle. The visualization snapshots confirm this behavior. On the contrary, if the polymer would have penetrated inside the hydrocarbon core then the SASA of the micellar aggregate would be greater in the ternary system. Clearly, as seen from Fig. 6, the difference between the SASA values in the binary and ternary systems increases with the concentration of the surfactant and aggregation number of the aggregate in solution.

3.7. Thermodynamics: enthalpy of solvation and aggregation

The solvation enthalpy was calculated using thermodynamic relations adopted from a previous implementation for aqueous solutions of amino acids[85] as given by eqn (S7)–(S11) in the ESI† section. The values are averaged over 10 ns of sampling time subsequent to the equilibrated trajectory of the final state of the solution (binary or ternary as it may be taken), and over 5 ns for the simulations of reference states (isolated PAA in a vacuum, and pure bulk water in the *NPT* ensemble), which is sufficient

Fig. 5 Aspect ratio (Φ) and eccentricity (e) of the micelles in the binary solution in the spherical micelle regime.
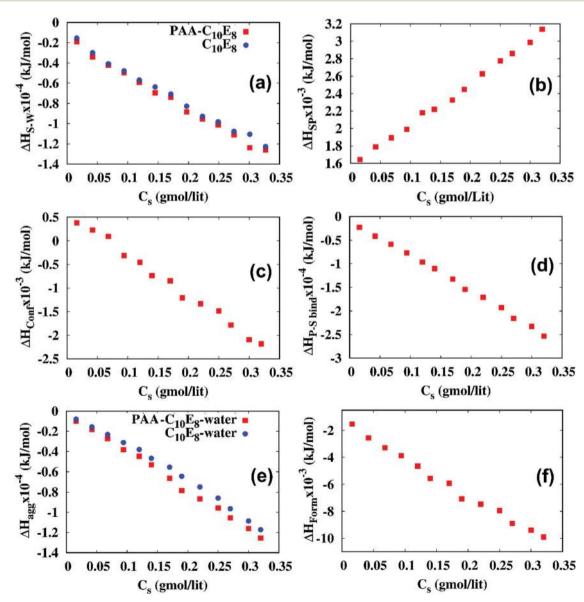

Fig. 6 Solvent accessible surface area (SASA) of the surfactant aggregates in the binary and ternary solution.

for sampling the reference states. The intermolecular potential energy of bulk water using the SPC model in the *NPT* ensemble was obtained as -40.8 kJ mol^{-1} in agreement with the reported value.[86]

In a similar manner, the total enthalpy of the binary surfactant–water solution, for each system, was obtained. The following quantities were calculated and are presented in Fig. 7 and Table 5S of the ESI:† (i and ii) the enthalpy of surfactant–water solvation (ΔH_{sol}) in the ternary and binary solutions, (iii) the enthalpy of solvation (ΔH_{sol}) of the polymer chain in the ternary solution, (iv) the enthalpy of formation of the ternary solution (ΔH_{form}), (v) the contribution of the conformational change of PAA to the enthalpy of solvation of PAA in the ternary solution (ΔH_{conf}), (vi) the enthalpy of polymer–surfactant binding in the ternary solution ($\Delta H_{P-S,bind}$), (vii) the enthalpy of

aggregation (ΔH_{agg}) of surfactant molecules in water, and (viii) the enthalpy of aggregation (ΔH_{agg}) of surfactant molecules in the ternary solution.

The analysis of the results on the basis of either the concentration of surfactant C_s or the aggregation number N_{agg} would be similar. ΔH_{sol} in the ternary and binary solutions becomes more favorable with an increase in C_s, driven by favorable surfactant–water interactions, which occurs even at low C_s. For the binary solution ΔH_{sol} decreases with an increase in C_s, which indicates that the favorable intermolecular interactions between the surfactant and water become stronger with an increase in C_s. As seen from Fig. 7(b), ΔH_{sol} of the polymer chain in the ternary solution becomes more endothermic (*i.e.* unfavorable) with an increase in the aggregation number. The interaction between PAA and the surfactant given by

Fig. 7 (a) Enthalpy of solvation interaction between the surfactant and water, (b) enthalpy of solvation interaction between the polymer and water, (c) conformation contribution to the enthalpy of solvation of the polymer, (d) enthalpy of binding between the polymer and surfactant, (e) aggregation enthalpy of the surfactant in water, and (f) enthalpy of formation of the ternary solution. The error values in the enthalpy calculations are less than 5%.

$\Delta H_{\text{P–S,bind}}$ is exothermic in the entire concentration range and increases with C_s. As seen from Fig. 7(c), the energetic contribution of the conformational change of PAA to the solvation enthalpy of the polymer in the ternary solution, ΔH_{conf}, is clearly exothermic for the entire range of C_s, with the exception of the very dilute conditions of $C_s \leq 0.07$ gmol l^{-1} (*i.e.* $N_{\text{agg}} \leq 21$). Interestingly, in the narrow concentration range 0.068 gmol l^{-1} < C_s < 0.094 gmol l^{-1} (21–29 for N_{agg}), there ΔH_{conf} shows a transition from endothermic to exothermic, which is directly associated with the transition from the micellar phase to the lamellar phase.

The data obtained on the enthalpy change of binding of the PAA chain to the aggregate, denoted by $\Delta H_{\text{P–S,bind}}$, with respect to the reference states of an isolated PAA chain in a vacuum and the surfactant–water binary solution, with the intermolecular interactions between the polymer and surfactant taken into account, is shown in Fig. 7(d). $\Delta H_{\text{P–S,bind}}$ is exothermic in the entire range with the behavior similar to that shown by ΔH_{conf}. Thus, the intermolecular interaction between PAA and the surfactant is conformationally cooperative in the entire concentration range.

The behavior of ΔH_{agg}, calculated as the enthalpy change for the formation of the surfactant aggregate with the reference states being the isolated surfactant molecules in a vacuum, denoted as ΔH_{agg}, in the ternary and binary solutions, is shown in Fig. 7(e). ΔH_{agg} is exothermic for all values of C_s in the binary and ternary solutions, which implies that aggregate formation is thermodynamically favored, as expected.[39] This result is in qualitative agreement with the theoretical model[39] of the free energy change of aggregation. The behavior as a function of C_s or N_{agg} is in agreement with the trend observed in an earlier study which showed that the free energy change is more exothermic at higher aggregation numbers.[39] As the entropy change for aggregation is positive (*i.e.* unfavorable), a negative change of the enthalpy of aggregation, wherein it is well-known that it has a dominant influence on the free energy change, would be in qualitative agreement with the negative free energy change (*i.e.* of being favorable) and its variation with the aggregation number, as known from previous studies[39,40] in the literature.

As shown in Fig. 7(f), the enthalpy of formation ΔH_{form} of the ternary solution is exothermic in the entire concentration range. Our simulations are able to thermodynamically describe the formation of the polymer–surfactant–water ternary solution of a non-ionic water-soluble polymer, a non-ionic surfactant, and water, as the results of the enthalpy change qualitatively mimic those of the free energy change, which, as expected, must be exothermic. The value of ΔH_{form} becomes more exothermic with an increase in C_s, which implies that the formation of lamellar aggregates in the PAA–C$_{10}$E$_8$–water system is more favored as compared to spherical micelles at those aggregation numbers. The micellar range does exist but it is confined to a shorter range ($N_{\text{agg}} = 5$, $C_s = 0.016$ to $N_{\text{agg}} = 21$, $C_s = 0.068$ mol l^{-1}) as compared to the range for the formation of the lamellar aggregate. While the data for ΔH_{form} of the binary (C$_{10}$E$_8$–water) solution is not provided here, it is important to note that the range for which spherical micelles exist is larger in the binary solution ($5 < N_{\text{agg}} < 37$) as compared to the ternary solution ($5 < N_{\text{agg}} < 21$). This portrays the situation of a lamellar aggregate being more favorable than a spherical micelle for the adsorption of a non-ionic polymer on a non-ionic surfactant aggregate, and for the formation of the ternary aqueous solution containing the polymer adsorbed on the surface of the surfactant aggregate. Therefore, clearly, the formation of lamellar aggregates is more favorable as compared to spherical micelles in the PAA–C$_{10}$E$_8$–water system at higher values of the aggregation number. These results are important as these are not known from experimental study[16] of this system.
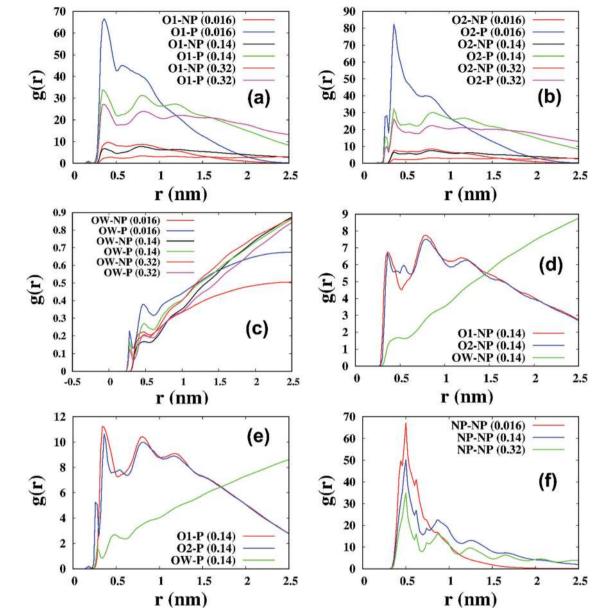
3.8. Structure of polymer–surfactant complexes

3.8.1. Radial distribution functions. The RDFs involving carbonyl oxygen (O1 of the C=O group of PAA), hydroxyl oxygen (O2 of the –OH group of PAA) and water oxygen (OW) with respect to the polar groups (ethylene oxide, EO) and non-polar groups (CH$_2$) of the C$_{10}$E$_8$ surfactant are shown in Fig. 8, and Fig. 7S–9S of the ESI† section. Here a non-polar group refers to those in the hydrocarbon tail of the surfactant consisting of carbon atoms (C1, C2, C3, C4, C5, C6, C7, C8, C9 and C10) and a polar moiety refers to ethylene oxide groups (Oa, C9, C10, Ob, C11, C12, Oc, C13, C14, Od, C15, C16, Oe, C17, C18, Of, C19, C20, Og, C21, C22, Oh, C23, C24, OS and HS). The atom names are specified as shown in Fig. 1. The peak position of the RDF of the O1–P pair is located at 0.33 nm and that of the O1–NP pair is at 0.39 nm for $C_s = 0.016$ mol l^{-1}. The peak position of the curve for the O2–P pair is at 0.26 nm and that of the O2–NP pair is at 0.36 nm for $C_s = 0.016$ mol l^{-1}. A similar structure is observed at higher aggregation number and surfactant concentration.

A comparison of the RDFs of carbonyl oxygen O1 (of C=O) with respect to the polar (EO) and non-polar (CH$_2$) groups of the surfactant, on the basis of the location of the first peak positions, shows that the polar EO groups are located closer to the O1 oxygens of PAA. A similar behavior of the structure is seen for the hydroxyl O2 oxygens of PAA. These values indicate that PAA interacts strongly with the polar groups of the surfactant aggregate as compared to the non-polar hydrocarbon groups, and it is adsorbed on the surface of the micelle. These RDFs indicate that the polymer chain positions itself near the polar groups of the surfactant chains and it is neither present at the hydrocarbon–water interface nor solubilized in the interior region of the micelle. This behavior, interestingly, is similar to the results and behavior of polyacrylate polyelectrolytes and uncharged PAA interacting with CTAC cationic surfactant micelles.[45]
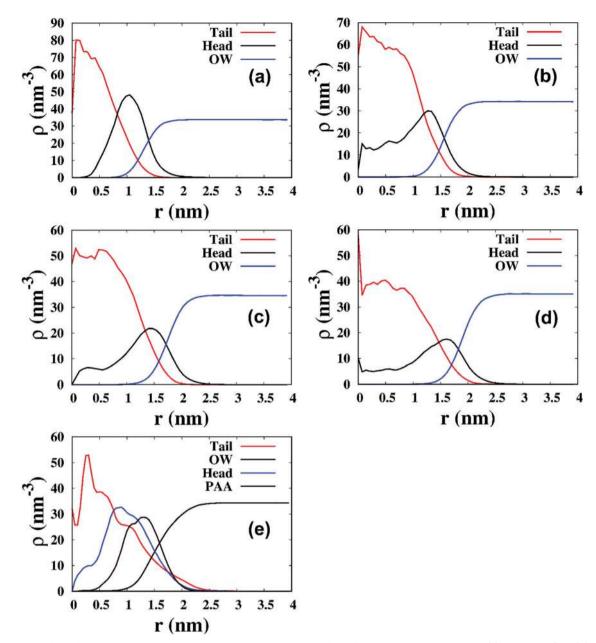
The RDFs shown in Fig. 8(c) indicate that water molecules interact favorably and preferentially with the polar groups rather than the non-polar groups of the surfactant. This is corroborated by the results of the density profile of water as shown in Fig. 9. This phenomenon is the hydrophobic effect,[24] which is the key driving force for the formation of such micelles. The non-polar groups of the surfactant avoid contact

Fig. 8 (a) RDFs for carbonyl oxygen (O1) of PAA with the polar (P) and non-polar (NP) parts of the surfactant in the ternary solution at different values of C_s. (b) RDFs for carbonyl oxygen (O2) of PAA with the polar (P) and non-polar (NP) parts of the surfactant in the ternary solution at different values of C_s. (c) RDFs for carbonyl oxygen (OW) of PAA with the polar (P) and non-polar parts (NP) of the surfactant in the ternary solution at different values of C_s. (d) RDFs of different oxygens with the non-polar parts (NP) of the surfactant at $C_s = 0.14$ gmol l^{-1} in the ternary solution. (e) RDFs of different oxygens with the polar parts (P) of the surfactant at $C_s = 0.14$ gmol l^{-1} in the ternary solution. (f) RDFs of the nonpolar parts (NP) with the nonpolar parts (NP) at different values of C_s.

with water molecules and cluster themselves to form the core region of the micelle. A comparison of the RDFs of CH$_2$ groups with respect to O1, O2 and OW (Fig. 8(d)) shows that distinct coordination peaks are present for O1 and O2 but not for OW, due to O1 and O2 being a chemically bonded part of the PAA chain, while water is kept away due to its hydrophilic nature. However, a comparison of the RDFs of the polar EO groups with respect to O1, O2 and OW (Fig. 8(e)) shows that distinct coordination peaks are present for all three types of oxygen, due to the polar nature of all these atoms and the hydrophilic nature of the EO groups. A comparison of

the RDFs of water oxygens OW with respect to the polar EO and the non-polar CH$_2$ groups of the surfactant, on the basis of the location of the first peak, shows that there is a distinct peak in the OW–EO RDF which is absent in the OW–CH$_2$ RDF. This indicates that water shows a clear first coordination shell for its interaction and structure with respect to the polar EO groups and does not exhibit this with respect to the non-polar CH$_2$ groups. The interaction of water with the hydrophobic CH$_2$ groups of the surfactant has a diffuse intermolecular structure. A comparison of the RDFs shown in Fig. 8(d) and (e) also indicates that, for the polar EO
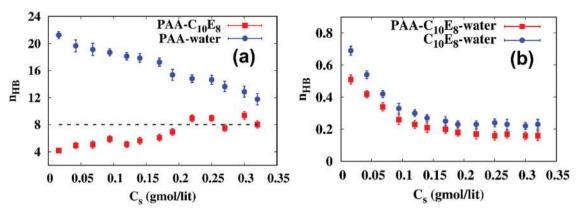
Fig. 9 Density profiles of the atoms and groups within the micellar aggregates for different aggregation numbers. (a) N_{agg} = 13, C_s = 0.042 gmol l^{-1} in the binary solution, (b) N_{agg} = 21, C_s = 0.068 gmol l^{-1} in the binary solution, (c) N_{agg} = 29, C_s = 0.094 gmol l^{-1} in the binary solution, (d) N_{agg} = 37, C_s = 0.12 gmol l^{-1} in the binary solution and (e) N_{agg} = 21, C_s = 0.068 gmol l^{-1} in the ternary solution.

group of the surfactant, the proximity (*i.e.* the intermolecular distance) of the peak positions follows the order: O2 < O1 < OW, while for the non-polar CH$_2$ group of the surfactant the proximity of the peak positions follow the order: O2 < O1. Therefore, the carbonyl oxygen as compared to the hydroxyl oxygen of PAA is closer to water oxygen.

3.8.2. Radial density profiles. The radial density profiles within the micelles are shown in Fig. 9. As shown in Fig. 9(e), for N_{agg} = 21 and C_s = 0.068 mol l^{-1}, the PAA chain is adsorbed on the surface of the micelle, favorably interacting with the polar and the non-polar groups of C$_{10}$E$_8$. Hydrophobic interactions and hydrogen bonding simultaneously aid the

formation of the polymer–surfactant complex. For micelles having a small value of N_{agg}, water molecules are able to easily penetrate into the micelle (Fig. 9(b) and (c)). Water penetrates inside the micelle for N_{agg} = 21 (C_s = 0.068 mol l^{-1}) but not for N_{agg} = 29 (C_s = 0.094 mol l^{-1}). It is clear that water shows some penetration into the hydrocarbon core. Water molecules are unable to penetrate inside the micelle at higher aggregation numbers and interact with only the polar EO groups of the surfactant. At low values of N_{agg} and C_s > CMC (N_{agg} = 5 and 13) the micelles formed are not structurally well-defined, with some of the hydrocarbon tails of the surfactant molecules being on the surface of the aggregate.

Fig. 10   (a) The PAA–$C_{10}E_8$ HB and PAA–water HB formed by the PAA chain in the ternary solution. HBs are formed between polar oxygens (Oa, Ob, Oc, Od, Oe, Of, Og, and Oh) of $C_{10}E_8$ and hydroxyl groups (O2, HA) of PAA, and between hydroxyl groups (O2, HA) of PAA and water. (b) Number of HBs between $C_{10}E_8$ and water in the ternary and binary solutions per EO group of the surfactant. The HBs occur between polar oxygens (Oa, Ob, Oc, Od, Oe, Of, Og, and Oh) of the surfactant and water. "HB" refers to hydrogen bonds.

3.9. Hydrogen bonding

It has been suggested[10,11] that hydrogen bonding is one of the key driving forces for the formation of polymer–surfactant complex aggregates of water soluble polymers. The structural criterion for the formation of hydrogen bonds (HBs) used in our simulations is as follows: a donor–acceptor distance less than 0.35 nm, and the hydrogen–donor–acceptor bond angle, *i.e.* H–O···O bond angle, must be less than 30°.[87] The interactions in the case of non-ionic surfactants come only from weak electrostatics, hydrogen bonding and van der Waals dispersion forces, with hydrogen bonding having a significant contribution among these. The different types of donor–acceptor pairs in the case of PAA interacting with water are known,[51] of which significant HBs are seen to occur between oxygens of the polar EO group and O2HA of PAA as shown by our simulations. The HBs between EO oxygens and O2HA of PAA obtained from the simulations are shown in Fig. 10. The number of these HBs increases with N_{agg} and C_s and this is the major contribution to H-bonding, as originally suggested[88] by an experimental study. The contribution of other types of HB is negligible and those values are calculated and shown in Fig. 11S–13S as ESI.† The PAA chain, by adopting an extended conformation, is able to interact more favorably and bind with surfactant molecules *via* hydrogen bonding at higher levels of C_s. For $N_{agg} > 61$, $C_s > 0.19$ mol l⁻¹ the number of HBs between PAA and the surfactant is almost constant, at a value of 8, which shows that at higher concentrations the PAA chain is saturated with surfactant molecules. At a maximum 8 HBs are formed, which specifically are: hydrogen bonds between O2HA of PAA and oxygens of the polar EO group, per PAA chain. The smallest number of HBs formed by the PAA chain is 4 at the smallest aggregation number 5 ($C_s = 0.016$ gmol l⁻¹), which is contributed by HBs between O2HA of PAA and oxygens of the polar EO groups. As seen from Fig. 10(a), the number of HBs between PAA and water decreases with an increase in N_{agg} and C_s.

A "free" PAA chain in water forms 2.6 HBs with water per COOH group,[50,51] while the PAA chain as part of the polymer–surfactant complex forms 0.7 to 0.4 HBs with water, as seen

from Fig. 10(a). At low values of N_{agg} or C_s the number of HBs between PAA and the surfactant is less, and hence PAA interacts more with water as compared to the surfactant. Whereas, at high values of N_{agg} or C_s, the PAA chain is saturated with surfactant molecules, and hence its interaction with water is reduced. The data on the number of HBs between the surfactant and water per EO group of $C_{10}E_8$ is given in Fig. 10(b). With an increase in N_{agg} or C_s, the number of EO groups exposed to water is reduced, and therefore the number of HBs decreases with an increase in N_{agg} or C_s in the binary as well as the ternary solution. The number of surfactant–water HBs is slightly higher in the binary solution.

3.10. Cooperativity between the polymer and surfactant

In the literature, the experimental studies of the PAA–$C_{10}E_8$–water system[16,17] and polymer–surfactant mixtures in solution mention "cooperativity" between the polymer and surfactant for aggregate formation, but do not provide any analysis or estimation of the mechanism. From our study it is observed that uncharged PAA adopts a coiled conformation in aqueous solution, and undergoes chain extension with an increase in the size of the aggregate. Also, the simulations show that the micellar aggregates are more spherical in the ternary system. These observations suggest that the interaction between the polymer and surfactant is cooperative. It is well-known from experiments that the mean value and distribution of the aggregation numbers of micelles are different in binary and ternary systems, and this could be a measure of polymer–surfactant cooperativity. However, this is difficult to capture using fully atomistic molecular dynamics simulations with explicit solvent due to the requirement of a prohibitively large box.

4. Conclusions

The molecular structure and dynamics of aqueous solutions containing poly(acrylic acid) PAA and octaethyleneglycol *n*-dodecyl ether ($C_{10}E_8$) surfactant were investigated using atomistic

molecular dynamics with explicit water molecules as a function of the concentration of the surfactant. The simulation results are in qualitative agreement with experimental results for this particular system. Spherical micelles and anisotropic lamellar aggregates are formed at lower and higher values of the surfactant concentration, respectively. The transition from the micelle phase to the lamellar phase in the binary solution is observed in the concentration or aggregation number range $0.12 \text{ mol l}^{-1} \leq C_s \leq 0.14 \text{ mol l}^{-1}$ (*i.e.* $37 \leq N_{agg} \leq 45$), whereas in the ternary solution this transition is observed in the range $0.068 \text{ mol l}^{-1} \leq C_s \leq 0.094 \text{ mol l}^{-1}$ ($21 \leq N_{agg} \leq 29$).

For smaller micelles that correspond to smaller values of N_{agg}, the PAA chain adsorbs on the micelle surface in a coiled conformation, while for larger micelles that correspond to larger values of the surfactant concentration, PAA adsorbs on the surface of the lamellar aggregate in an extended conformation. The range of aggregation numbers in which micelles are formed in the ternary PAA–$C_{10}E_8$–water solution is smaller as compared to the range observed in the binary $C_{10}E_8$–water solution. Even at low C_s, the $C_{10}E_8$ molecules interact with the PAA chain, in agreement with experimental data on this system. The values of the aspect ratio Φ and eccentricity e for the micelle aggregates in the binary solution are greater than the values obtained in the ternary solution, which indicates that the micelle aggregates in the ternary solution are more spherical as compared to those formed in the binary $C_{10}E_8$–water solution, due to their strong favorable interaction with the PAA chain.

Strong favorable interactions between –COOH groups of PAA and EO groups of $C_{10}E_8$ occur, which facilitates polymer–surfactant interactions in solution as well as adsorption of PAA on surfactant aggregates. This result is supported by computational analysis using RDFs, the solvent accessible surface area (SASA) and atom density profiles. The SASA value of the aggregate in the binary ($C_{10}E_8$–water) solution is larger than the value obtained for the ternary system, and so the PAA chain adsorbs on the surface of the aggregate. PAA not only interacts with polar moieties but also with non-polar moieties of the surfactant. The adsorption of PAA on the $C_{10}E_8$ aggregate is driven by hydrogen bonding between carboxylic acid groups of PAA and EO groups of the surfactant. Interestingly, our simulations show that there is a clear transition in the radius-of-gyration $\langle R_g \rangle$ of the PAA chain adsorbed on the aggregate, in going from the spherical micellar regime to the lamellar aggregate regime. The adsorption and coiling of the PAA chain on the micelle are driven by the formation of stable hydrogen bonds between carboxylic acid groups of the PAA chain and EO groups of the $C_{10}E_8$ surfactant. At a low concentration of the $C_{10}E_8$ surfactant, the water molecules are able to interact with the hydrocarbon core of the micelle. However, at higher concentrations the water molecules are unable to penetrate into the hydrocarbon core, while interacting only with the polar moieties of the surfactant molecules. The polymer chain is able to interact more favorably to bind with surfactant molecules *via* hydrogen bonding at higher surfactant concentration, as the PAA chain adopts an extended conformation.

The solvation enthalpy of the $C_{10}E_8$ surfactant in the ternary PAA–$C_{10}E_8$–water solution indicates that a favorable interaction of water with $C_{10}E_8$ occurs even at low C_s. For large values of N_{agg} the PAA chain is able to interact more favorably and bind *via* hydrogen bonding, as it adopts an extended conformation. The intermolecular interaction between PAA and the surfactant is conformationally cooperative in the entire range of surfactant concentration investigated in this study. At higher concentrations of $C_{10}E_8$ the PAA chain is saturated with surfactant molecules.

The values of the enthalpy of surfactant aggregation show that aggregation is favored in the entire range of concentrations investigated in this study. The number of hydrogen bonds formed between PAA and surfactant molecules increases with C_s and attains a constant value. The enthalpy of formation of the ternary solution, which is exothermic in the entire concentration range, indicates that the formation of lamellar aggregates is more favorable than spherical micelles. These new structural and thermodynamic results are crucial in furthering our understanding of such systems, and for promoting new experimental studies which are absent in the field. The information obtained from the simulations is in agreement with experimental data available on these systems, and additionally the results presented in this study provide new insights into the molecular level structural and thermodynamic aspects of the micelles, surfactant aggregates and polymer–surfactant complexes in aqueous solutions of non-ionic surfactants and polymers.

Conflicts of interest

There are no conflicts to declare.

Acknowledgements

References

1   B. Jonnson, B. Lindman, K. Holmberg and B. Kronberg, *Surfactants and Polymers in Aqueous Solution*, John Wiley and Sons: Chichester, UK, 1998.

2   J. C. T. Kwak, *Polymer–Surfactant Systems, Surfactant Science Series 77; Ed.*, Marcel Dekker, New York, 1998.

3   C. L. Cooper, P. L. Dubin, A. B. Kayitmazer and S. Turksen, Polyelectrolyte-protein complexes, *Curr. Opin. Colloid Interface Sci.*, 2005, **10**, 52–78.

4   E. D. Goddard and K. P. Ananthapadmanabhan, *Interactions of Surfactants with Polymers and Proteins*, CRC Press, Boca Raton, FL, 1993.

5 S. K. Tripathy, J. Kumar and H. S. Nalwa, *Polyelectrolyte-surfactant interactions in handbook of polyelectrolytes and their applications*, American Science Publishers, Stevenson Ranch, CA, 2002.

6 M. J. Schick, *Nonionic surfactants: physical chemistry*, CRC Press, 1987.

7 P. Hansson and B. Lindman, Surfactant-polymer Interactions, *Curr. Opin. Colloid Interface Sci.*, 1996, **1**, 604–613.

8 P. Hansson, Interaction between polyelectrolyte gels and surfactants of opposite charge, *Curr. Opin. Colloid Interface Sci.*, 2006, **11**, 351–362.

9 R. Dong and J. Hao, Complex fluids of poly(oxyethylene) monoalkyl ether nonionic surfactants, *Chem. Rev.*, 2010, **110**, 4978–5022.

10 S. Saito, Binding of surfactants by polymers, *J. Colloid Interface Sci.*, 1960, **15**, 283–286.

11 S. Saito and T. Taniguichi, Effect of non-ionic surfactants on aqueous poly(acrylic acid) solutions, *J. Colloid Interface Sci.*, 1973, **44**, 114–120.

12 D. J. Mitchell, G. J. Tiddy, L. Waring, T. Bostock and M. P. McDonald, Phase behaviour of polyoxyethylene surfactants with water. Mesophase structures and partial miscibility (cloud points), *J. Chem. Soc., Faraday Trans. 1*, 1983, **79**, 975–1000.

13 K. Esumi and M. Ueno, *Structure-performance relationships in surfactants*, CRC Press, 2003.

14 M. Vasilescu, D. F. Anghel, M. Almgren, P. Hansson and S. Saito, Fluorescence study of the interactions between non-ionic poly(ethylene oxide) surfactants and poly(acrylic acid) in aqueous solutions, *Langmuir*, 1997, **13**, 6951–6955.

15 D. F. Anghel, S. Saito, A. Iovescu, A. Baran and M. Cornitescu, The aggregation of non-ionic surfactants in presence of Poly(methacrylic acid), *Colloid Polym. Sci.*, 2007, **285**, 771–779.

16 D. F. Anghel, S. Saito, A. Baran and A. Iovescu, Interactions between poly(acrylic acid) and non-ionic surfactants with the same poly(ethylene oxide) but different hydrophobic moieties, *Langmuir*, 1998, **14**, 5342–5346.

17 D. F. Anghel, S. Saito, A. Iovescu and A. Baran, Some critical points in the interaction between homogeneous non-ionic surfactant and poly(acrylic acid), *Colloids Surf., A*, 1994, **90**, 89–94.

18 E. D. Errico, D. Ciccarelli, O. Ortana, L. Paduano and R. Sartorio, Interaction between pentaethylene glycol *n*-octyl ether and Low molecular weight Poly(acrylic acid), *J. Colloid Interface Sci.*, 2004, **270**, 490–495.

19 E. D. Errico, D. Ciccarelli, O. Ortana, L. Paduano and R. Sartorio, Interaction between pentaethylene glycol *n*-octyl ether and poly(acrylic acid): effect of the polymer molecular weight, *J. Colloid Interface Sci.*, 2007, **314**, 242–250.

20 C. Maloney and K. Huber, Mixtures of polyacrylic acid and non-ionic surfactant at the water/air interface, *J. Colloid Interface Sci.*, 1994, **164**, 463–470.

21 S. Saito, Properties of nonionic surfactant-polymethacrylic acid complexes: comparison with the polyacrylic acid complexes, *J. Colloid Interface Sci.*, 1994, **165**, 505–511.

22 H. Fujimatsu, S. Ogasawara and S. Kuroiwa, Lower critical solution temperature and theta temperatures of aqueous solutions of non-ionic surface active agents of various poly oxyethylene chain lengths, *Colloid Polym. Sci.*, 1988, **266**, 594–600.

23 K. Hubert and R. Heinz, Molecular Dynamics Computer simulations of surfactant Monolayers: Monododecyl Pentaethylene Glycol at surface between air and water, *J. Phys. Chem. B*, 1999, **103**, 8493–8501.

24 C. Tanford, *The hydrophobic effect: formation of micelles and biological membranes*, J. Wiley, 2nd edn, 1980.

25 P. C. Hiemenz and R. Rajagopalan, *Principles of Colloid and Surface Chemistry*. Marcel Dekker. Inc, New York, 1997.

26 M. J. Rosen and J. T. Kunjappu, *Surfactants and interfacial phenomena*. J. Wiley, 2012.

27 B. Smit, P. A. J. Hilbers, K. Esselink, L. A. M. Rupert, N. M. van Oss and A. G. Schlijper, Structure of a water/oil interface in the presence of micelles: a computer simulation study, *J. Phys. Chem.*, 1991, **95**, 6361–6368.

28 M. A. Floriano, E. Caponetti and A. Z. Panagiotopoulos, Micellization in model surfactant systems, *Langmuir*, 1999, **15**, 3143–3151.

29 J. C. Shelley and M. Y. Shelley, Computer simulation of surfactant solutions, *Curr. Opin. Colloid Interface Sci.*, 2000, **5**, 101–110.

30 R. D. Groot, Mesoscopic simulation of polymer–surfactant aggregation, *Langmuir*, 2000, **16**, 7493–7502.

31 S. Garde, L. U. Yang, J. S. Dordick and M. E. Paulaitis, Molecular dynamic simulations of C_8E_5 micelle in explicit water structure and hydrophobic solvation thermodynamics, *Mol. Phys.*, 2002, **100**, 2299–2306.

32 S. Abel, M. Waks, M. Massimo and W. Urbach, Effect of surfactant conformation on structure of small size non-ionic reverse micelles: a molecular dynamics study, *Langmuir*, 2006, **22**, 9112–9120.

33 S. Karaborni, N. M. Van Os, K. Esselink and P. A. J. Hilbers, Molecular dynamics simulations of oil solubilization in surfactant solutions, *Langmuir*, 1993, **9**, 1175–1178.

34 S. Karaborni and B. Smit, Computer simulations of surfactant structures, *Curr. Opin. Colloid Interface Sci.*, 1996, **1**, 411–415.

35 M. Tarek, S. Bandyopadhyay and M. L. Klein, Molecular dynamics studies of aqueous surfactants systems, *J. Mol. Liq.*, 1998, **78**, 1–6.

36 K. Esselink, P. A. J. Hilbers, N. M. Van Os, B. Smit and S. Karaborni, Molecular dynamics simulations of model oil/water/surfactant systems, *Colloids Surf., A*, 1994, **91**, 155–167.

37 M. Laradji, O. G. Mouritsen, S. Toxvaerd and M. J. Zuckermann, Molecular dynamics simulations of phase separation in the presence of surfactants, *Phys. Rev. E: Stat., Nonlinear, Soft Matter Phys.*, 1994, **50**, 1243–1253.

38 E. Ruckenstein and R. Nagarajan, Relation between the transition point in micellar size distribution, the CMC, and the cooperativity of micellization, *J. Colloid Interface Sci.*, 1983, **91**, 500–506.

39 E. Ruckenstein and R. Nagarajan, Theory of surfactant self-assembly: a predictive molecular thermodynamic approach, *Langmuir*, 1991, **7**, 2934–2969.

40 R. Nagarajan, Thermodynamics of nonionic polymer–micelle association, *Colloids Surf.*, 1985, **13**, 1–17.

41 S. Puvvada and D. Blankschtein, Thermodynamic description of micellization, phase behavior, and phase separation of aqueous solutions of surfactant mixtures, *J. Phys. Chem.*, 1992, **96**, 5567–5579.

42 S. Puvvada and D. Blankschtein, Molecular-thermodynamic approach used to predict micellization, phase behavior, and phase separation of micellar solutions, *Langmuir*, 1990, **6**, 894–895.

43 Y. J. Nikas and D. Blankschtein, Complexation of nonionic polymers and surfactants in dilute aqueous solutions, *Langmuir*, 1994, **10**, 3512–3528.

44 A. Shiloach and D. Blankschtein, Predicting micellar solution properties of binary surfactant mixtures, *Langmuir*, 1998, **14**, 1618–1636.

45 M. S. Sulatha and U. Natarajan, Molecular dynamics simulations of adsorption of poly-(acrylic acid) and poly-(methacrylic acid) on dodecyltrimethylammonium chloride micelle in water: effect of charge density, *J. Phys. Chem. B*, 2015, **119**, 12526–12539.

46 S. Hu, Q. Zhu, P. Wang, H. Wang, C. Li and S. Sun, Effect of HPAM hydrolysis degree on cationic mixtures of DTAB/HPAM: a coarse-grained molecular dynamic simulation, *Comput. Mater. Sci.*, 2018, **153**, 134–140.

47 B. Z. Shang, Z. Wang and R. G. Larson, Molecular dynamics simulations of Interactions between a sodium dodecyl sulfate micelle and polyethylene oxide polymer, *J. Phys. Chem. B*, 2008, **112**, 2888–2900.

48 B. Hess, C. Kutzner, D. van der Spoel and E. Lindahl, GROMACS4: algorithms for highly efficient load balanced and scalable molecular simulation, *J. Chem. Theory Comput.*, 2008, **4**, 435–447.

49 L. D. Schuler, X. Daura and W. F. van Gunsteren, An Improved GROMOS96 force field for Aliphatic Hydrocarbons in the condensed phase, *J. Comput. Chem.*, 2001, **22**, 1205–1218.

50 M. S. Sulatha and U. Natarajan, Origin of the difference in structural behavior of poly(acrylic acid) and poly-(methacrylic acid) in aqueous solution discerned by explicit-solvent explicit-ion MD simulations, *Ind. Eng. Chem. Res.*, 2011, **50**, 11785–11796.

51 B. Li, L. Xu, Q. Wu, T. Chen, P. Sun, Q. Jin, D. Ding, X. Wang, G. Xue and A. Shi, Various types of hydrogen bonds, their temperature dependence and water–polymer interaction in hydrated poly(acrylic acid) as revealed by ^{1}H solid state NMR spectroscopy, *Macromolecules*, 2007, **40**, 5776–5786.

52 M. S. Sulatha and U. Natarajan, Molecular dynamics simulations of PAA–PMA polyelectrolyte copolymers in dilute aqueous solution: chain conformations and hydration properties, *Ind. Eng. Chem. Res.*, 2012, **51**, 10833–10839.

53 G. Yao, J. Zhao, S. B. Ramisetti and D. Wen, Atomistic molecular dynamic simulation of dilute poly(acrylic acid) solution: Effects of simulation size sensitivity and ionic strength, *Ind. Eng. Chem. Res.*, 2018, **57**, 17129–17141.

54 R. Chockalingam and U. Natarajan, Molecular Dynamics Simulations Investigation of Structure and Thermodynamic Properties of Symmetric Poly(styrene-*block*-acrylic acid)-(PS-*b*-PAA) Micelle in Salt-Free Aqueous Solution, *Macromol. Theory Simul.*, 2015, **24**, 580–594.

55 R. Chockalingam and U. Natarajan, Structure and solvation thermodynamics of asymmetric poly(acrylic acid)-*b*-polystyrene polyelectrolyte block copolymer micelle in water: effect of charge density and chemical composition, *Polymer*, 2018, **158**, 103–119.

56 P. Bacle, M. Jardat, V. Marry, G. Mériguet, G. Batôt and V. Dahirel, Coarse-grained models of aqueous solutions of polyelectrolytes: significance of explicit charges, *J. Phys. Chem. B*, 2019, **124**, 288–301.

57 A. P. Heiner, L. Kuutti and O. Teleman, Comparison of the interface between water and four surfaces of native crystalline cellulose by molecular dynamics simulations, *Carbohydr. Res.*, 1998, **306**, 205–220.

58 A. E. Mark, S. P. van Helden, P. E. Smith, L. H. M. Janssen and W. F. van Gunsteren, Convergence properties of free energy calculations: α-cyclodextrin complexes as a case study, *J. Am. Chem. Soc.*, 1994, **116**, 6293–6302.

59 *Materials Studio*, Accelerys Software Inc., San Diego, CA.

60 J. P. Ryckaert and A. Bellemans, Molecular dynamics of liquid butane near its boiling point, *Chem. Phys. Lett.*, 1975, **30**, 123–125.

61 I. G. Tironi, R. Sperb, E. P. Smith and V. W. F. Gunsteren, A generalized reaction field method for molecular dynamics simulations, *J. Chem. Phys.*, 1995, **102**, 5451–5459.

62 K. Devanand and J. C. Selser, Asymptotic behavior and long-range interactions in aqueous solutions of poly(ethy1ene oxide), *Macromolecules*, 1991, **24**, 5943–5947.

63 W. L. Jorgensen, J. Chandrasekhar, J. D. Madura, R. W. Impey and M. L. Klein, Comparison of simple potential functions for simulating liquid water, *J. Chem. Phys.*, 1983, **79**, 926–935.

64 H. Berendsen, J. P. M. Postma, W. F. van Gunsteren and J. Hermans, *Intermolecular Forces*, ed. Pullman, B., Reidel, Dordrecht, The Netherlands, 1981, pp. 331–342.

65 D. van der Spoel, P. J. van Mareen and J. C. A. Berendsen, systematic study of water models for molecular simulation: derivation of water models optimized for use with reaction field, *J. Chem. Phys.*, 1998, **108**, 10220.

66 R. H. Henchman, Free energy of liquid water from a computer simulation via cell theory, *J. Chem. Phys.*, 2007, **126**, 064504.

67 R. Chockalingam and U. Natarajan, Dynamics of conformations, hydrogen bonds and translational diffusion of poly(methacrylic acid) in aqueous solution and the concentration transition in MD simulations, *Mol. Phys.*, 2015, **113**, 3370–3382.

68 P. Sappidi and U. Natarajan, Factors responsible for the aggregation behavior of hydrophobic polyelectrolyte PEA in aqueous solution studied by molecular dynamics simulations, *J. Mol. Graphics Modell.*, 2017, **75**, 306–315.

69 D. G. Mintis and V. G. Mavrantzas, Effect of pH and molecular length on the structure and dynamics of short poly(acrylic acid) in dilute solution: detailed molecular dynamics study, *J. Phys. Chem. B*, 2019, **123**, 4204–4219.

70 D. van der Spoel and P. J. van Maaren, The origin of layer structure artifacts in simulations of liquid water, *J. Chem. Theory Comput.*, 2006, **2**, 1–11.

71 B. Hess, H. J. C. Bekker and J. G. E. M. Fraaije, LINCS: a linear constraint solver for molecular simulations, *J. Comput. Chem.*, 1997, **18**, 1463–1472.

72 G. Bussi, D. Donadio and M. Parrinello, Canonical sampling through velocity rescaling, *J. Chem. Phys.*, 2007, **126**, 014101.

73 H. J. C. Berendsen, J. P. M. Postma, V. W. F. Gunsteren, A. DiNola and J. R. Haak, Molecular dynamics with coupling to an external bath, *J. Chem. Phys.*, 1984, **81**, 3684–3690.

74 H. Lee, Effect of polyelectrolyte size on multilayer conformation and dynamics at different temperatures and salt concentrations, *J. Mol. Graphics Modell.*, 2016, **70**, 246–252.

75 K. A. Beauchamp, Y. S. Lin, R. Das and V. S. Pande, Are protein force fields getting better? A systematic benchmark on 524 diverse NMR measurements, *J. Chem. Theory Comput.*, 2012, **8**, 1409–1414.

76 H. Eslami, F. Mozaffari, J. Moghadasi and F. Müller-Plathe, Molecular dynamics simulation of confined fluids in isosurface–isothermal–isobaric ensemble, *J. Chem. Phys.*, 2008, **129**, 194702–194710.

77 J. E. Basconi and M. R. Shirts, Effects of temperature control algorithms on transport properties and kinetics in molecular dynamics simulations, *J. Chem. Theory Comput.*, 2013, **9**, 2887–2899.

78 U. W. Suter and P. J. Flory, Conformational energy and configurational statistics of polypropylene, *Macromolecules*, 1975, **8**, 765–776.

79 U. W. Suter, Epimerisation of vinyl polymer to stereochemical equilibrium, *Macromolecules*, 1981, **14**, 523–528.

80 E. Chiessi and G. Paradossi, Influence of tacticity on hydrophobicity of poly(*N*-isopropylacrylamide): a single chain molecular dynamics simulation study, *J. Phys. Chem. B*, 2016, **120**, 3765–3776.

81 S. Miyamoto and P. A. Kollman, SETTLE: An analytical version of the SHAKE and RATTLE algorithm for rigid water models, *J. Comput. Chem.*, 1992, **13**, 952–962.

82 M. Jorge, Molecular dynamics simulations of self-assembly of *n*-decyltrimethyammonium bromide micelles, *Langmuir*, 2008, **24**, 5714–5725.

83 C. D. Bruce, M. L. Berkowitz, L. Perera and D. E. Forbes, Molecular dynamics simulation of sodium dodecyl sulfate micelle in water: micellar structural characteristics and counter-ion distribution, *J. Phys. Chem. B*, 2002, **106**, 3788–3793.

84 F. Eisenhaber, P. Lijnzaad, P. Argos, C. Sander and M. Scharf, The double cubic lattice method: efficient approaches to numerical integration of surface area and volume and to dot surface contouring of molecular assemblies, *J. Comput. Chem.*, 1995, **16**, 273–284.

85 B. Hess and N. F. van der Vegt, Hydration thermodynamic properties of amino acid analogues: a systematic comparison of biomolecular force fields and water models, *J. Phys. Chem. B*, 2006, **110**, 17616–17626.

86 H. J. C. Berendsen, J. R. Grigera and T. P. Straatsma, The missing term in effective pair potentials, *J. Phys. Chem.*, 1987, **91**, 6269–6271.

87 A. J. Luzar, Resolving the hydrogen bond dynamics conundrum, *J. Chem. Phys.*, 2000, **113**, 10663–10675.

88 I. D. Robb and P. Stevenson, Interaction between poly(acrylic acid) and an ethoxylated nonionic surfactant, *Langmuir*, 2000, **16**, 7168–7172.